Fuel 280 (2020) 118631

Contents lists available at ScienceDirect

Fuel

journal homepage: www.elsevier.com/locate/fuel

Full Length Article

Transmission of trace metals from fuels to soot particles: An ICP-MS and soot nanostructural disorder study using diesel and diesel/Karanja biodiesel blend

Pranay P. Morajkar[a,b,1], Moataz K. Abdrabou[a,1], Abhijeet Raj[a,c,*], Mirella Elkadi[d], Sasi Stephen[d], Mohamed Ibrahim Ali[e]

[a] Department of Chemical Engineering, Khalifa University of Science and Technology, Abu Dhabi, United Arab Emirates
[b] School of Chemical Sciences, Goa University, Taleigao Plateau, Goa, India
[c] Centre for Catalysis and Separation, Khalifa University of Science and Technology, Abu Dhabi, United Arab Emirates
[d] Department of Chemistry, Khalifa University of Science and Technology, Abu Dhabi, United Arab Emirates
[e] Department of Mechanical Engineering, Khalifa University of Science and Technology, Abu Dhabi, United Arab Emirates

ARTICLE INFO

Keywords:
Metals transmission
Karanja biodiesel
ICP-MS
Soot Nanostructure
Crystal disorder

ABSTRACT

Despite benefits of biodiesel such as reduced soot emissions and enhanced combustion efficiency, it enhances NOx emissions and may emit toxic trace metals that are present in biomass. This investigation focuses on the transmission of trace metals from fuels (diesel, Karanja biodiesel, and diesel/biodiesel blend) to soots generated from them. The study finds that the addition of 20% Karanja-biodiesel to diesel enhances the transmission of toxic metals such as Zn, Sr, Cs, and Pb to soot by normalized factors, defined as the ratio of the transmission rate from diesel to its soot (%) and the transmission rate from blended fuel to its soot (%), of 17, 7, 58 and 3, respectively, as compared to diesel. Although Cu and Fe were dominant metals in diesel and its soot, their transmission from fuel to soot was only 0.09%, suggesting a preferential selectivity of some metals such as Zn, Sr, Cs, and Pb or the catalytic effects of some metals such as Fe and Cu on soot surface. The nanostructural investigation of soot using HRTEM, XRD, and Raman analyses confirm that the addition of Karanja biodiesel to diesel induces structural disorders in soot such as higher fringe tortuosity, shorter fringe length, and smaller primary particle diameter than diesel soot that enhance its reactivity and possibly the trapping efficiency of metals. A combination of greater degree of metal transmission from Karanja biodiesel-blended diesel fuel to soot and the increased nanostructural disorder and reactivity makes soot from such blend potentially more hazardous than diesel soot.

1. Introduction

Harvesting sustainable sources of energy is a crucial factor for the growth and development of countries especially that the demand for energy is inevitably increasing with time and population growth. According to the recent projections of the International Energy Agency, the consumptions of biofuels will increase from about 2 million barrels of oil equivalent per day in 2019 to 4.6 million barrels of oil equivalent per day in 2040 [1,2]. As a result of the considerable growth in the modern use of bioenergy and biofuels, the share of biofuels in global energy supply is expected to increase by 60% and reach nearly 940 Mtoe in 2040 [1]. Unlike diesel, biodiesels have oxygen in their molecular structure with considerably lower sulfur and aromatic content, higher cetane number, higher biodegradability, higher flash point, and inherent lubricity [3].

One of the prominent examples of biofuels is the non-edible oil, Karanja oil (pongamia pinnata), which is known to be one of the few tree-borne seed oils that can be used to produce biodiesel. This biofuel source can easily be cultivated at low cost on any type of soil, as they require minimum amount of moisture and resources [4], and its biodiesel comes into compliance with ASTM D-6751 [5]. Small quantities of biodiesel (5–20 vol%) blended with diesel are the most common blends, as they do not require any engine modifications and are identified as B5 to B20 [6], with B20 being the most efficient biodiesel blend ratio identified so far in the literature. The combustion of biodiesel in compression ignition engines can reduce smoke, PM, carbon monoxide

* Corresponding author at: Department of Chemical Engineering, Khalifa University of Science and Technology, Abu Dhabi, United Arab Emirates.
E-mail address: abhijeet.raj@ku.ac.ae (A. Raj).
[1] Equal contribution by first two authors.

https://doi.org/10.1016/j.fuel.2020.118631
Received 10 May 2020; Received in revised form 24 June 2020; Accepted 3 July 2020

(CO), and unburned hydrocarbon (HC) emissions [7]. In spite of the numerous benefits of the utilization of biodiesel, the combustion of biodiesel is still associated with other critical problems such as the increased emission of nitrogen oxides (NOx) [8]. PM emission raises a serious concern for the human health not only due its effect on the respiratory system, but also due to the presence of toxic substances and trace metals embedded in it [9]. Since biofuels are extracted from plants grown in certain rural areas, their chemical composition varies and might contain some hazardous components. For example, organometallic complexes are inherently present in plant derived oils. Despite of distillation and other separation pre-processing steps, many of these metallic complexes or ions get dissolved in biofuels [10]. Such metallic constituents and ions may get transmitted into the environment either directly as metal complexes/oxides or via PM. Heavy metals associated with respirable particles have also been shown to increase lung or cardiopulmonary problems [11]. Some of the critical metal elements that are of primary concern for a variety of human health-related and natural environment problems includes arsenic (As), cadmium (Cd), chromium (Cr), copper (Cu), lead (Pb), mercury (Hg), nickel (Ni), aluminum (Al), manganese (Mn), vanadium (V), and zinc (Zn) [12]. Their potential hazards are well documented and guidelines are provided by the World Health Organization. According to the Environmental Protection Agency (EPA), the combustion of fossil fuels dominantly results in the release of gaseous pollutants such as CO, CO_2, NOx, and unburnt hydrocarbons, which are known to alter the atmospheric radical budget [13]. It has now been established that, apart from the gaseous pollutants, diesel combustion also serves as the principal anthropogenic source of trace metals such as Be, Co, Hg, Mo, Ni, Se, Sn, and V [14]. Fossil fuel (especially diesel) combustion also contributes to the concentrations of hazardous metals such as arsenic, chromium, copper, manganese, and zinc in the atmosphere, though a large percentage of arsenic, cadmium, copper, nickel, and zinc are usually emitted from industrial metallurgical processes in the form of PM of various sizes [15]. Furthermore, in a study on trace metals in PM performed in the Detroit urban atmosphere, Utsunomiya et al. concluded that the toxicity of the trace metals significantly increases, as they become a part of fine PM and are more easily breathable by living organisms [16]. Significant concentrations of heavy metals are reported to be present in PM with size < 2.5 μm. Such particles when enter into lungs, they are known to induce oxidative stress [17,18]. For a more detailed guideline on the trace metal's acceptable emissions levels, a list of the most significant trace metals that are commonly released by the diesel fuel and some information on them are provided in Table 1. The main metal constituents were identified by characterizing soot using Inductively Coupled Plasma-Atomic Emission Spectrometry (ICP-AES), while their corresponding average concentrations in the atmosphere and their time weighted threshold levels are the suggested values by the EPA [15].

Several studies in the literature have investigated the trace metal content in the PM and their concentrations in the atmosphere. For instance, Lee and Hieu [19] studied the PM heavy metal composition and the effect of the weather change on the PM concentrations at several locations in Korea. Their research concluded that the higher the temperature, the higher is the liberation of the metal components to the gaseous phase. It was revealed in their study that almost all of the metals constituents in PM had lower concentrations in the summer season as compared to spring. Ahmed et al. [9] demonstrated a study in Malaysia that focused on the analysis of trace metals in atmospheric PM during biomass burning haze episode that occurred in Southeast Asia in August 2015. The study utilized the inductively coupled plasma - mass spectrometry (ICP-MS) technique to analyze the metal composition of the PM. They reported that the concentrations of several metal constituents were beyond the allowable limits set by the local authorities. Corbin et al. [20] studied the toxic heavy metals that are being released via PM through the combustion of fuel oil in marine engines. They utilized the inductively coupled plasma - optical emission spectrometry (ICP-OES) technique to analyze the PM, and identified that the released metal components were mainly in the form of metal oxides. Moreover, the most hazardous metal constituent identified in soot was Vanadium due to its lower nucleation/condensation temperature. Dore et al. [21], with the aid of an atmospheric transport model, found that one of the major sources of trace metals in the atmosphere is through the emission of biomass PM. It is interesting to note that although many studies investigated the trace metal content in the PM and the fuel/biofuels independently, there are no reports regarding the relative transmission of metallic constituents from fuels, especially biodiesel blended fuels, to PM or soot. Moreover, the transmission rate of a particular metal from a fuel into soot could be influenced by the reactivity of PM or its nanostructural characteristics and active centers reacting with specific group of metal ions during combustion. The addition of biodiesel to diesel could further influence the soot reactivity and metal transmission into soot, and such effects need to be investigated. In addition, the metallic constituents in soot can induce its catalytic oxidation. While greater oxidative reactivity of soot due to enhanced nanostructural disorder is a positive factor for improved diesel particulate filter regeneration, such highly disordered and reactive soot containing metal ions/oxide constituents, if emitted directly to the environment, would be extremely toxic and hazardous to living organisms [22]. Therefore, it becomes extremely important to quantify the transmission percentage and distribution of metal constituents in soot generated from the combustion of biodiesel-diesel blends. The present investigation aims to provide an insight into the effects of biodiesel addition to diesel on metal transmission potential and nanostructural disorder in soot. A detailed analysis of the transmission of trace metals to the PM is performed using Karanja biodiesel-diesel blend and pure diesel fuels with the help of high resolution ICP-MS technique. The influence on the soot nanostructural disorder due to biodiesel blending has been investigated through high-resolution transmission electron microscopy (HRTEM), X-ray diffraction (XRD), and Raman spectroscopy analyses, and the results are discussed in the subsequent sections.

Table 1
Threshold limit values (TLV) for trace metals of concern adapted from EPA [15].

Trace metal	EPA TLV (8-hr TWA) in ppb	Ambient Air concentration in ppb	Hazardous Pollutants as per EPA	Carcinogenic	Human organs subject to Cancer
Cu	1	0.003	No	No	N/A
Fe	–	0.0016	No	Possible	DNA damage
Zn	–	0.015	No	No	N/A
Cr	1	0.003	Yes	Yes	Lungs
Pb	50	0.006	Yes	No	N/A
Mn	5000	0.020	Yes	No	N/A
V	50	0.003	No	Yes	DNA damage
Ni	1000	0.003–0.03	Yes	Yes	DNA damage
As	10	0.002	Yes	Yes	Lungs, Skin, Liver, Bladder
Co	0.10	0.0004	Yes	No	N/A

Table 2
Physical Properties of the tested fuels.

Physical properties	Diesel	Karanja biodiesel/diesel Blend (B20K)
Density (kg/m^3)	829	840
Dynamic viscosity (Kg/m.s)	0.00289	0.00295
Kinematic viscosity (mm^2/s) @ 20C	3.49	3.51
Cetane Number	59.7	62.1
Molecular weight, g/mol	197	336.14

2. Experimental methodology

2.1. Fuel preparation and physical properties

The commercial diesel fuel (Grade No. 2-D S15, ASTM D975 [23]) was obtained from a local fuel station in Abu Dhabi, UAE, and the Karanja biodiesel was purchased from SVM Agro processor, India. The Stabinger Viscometer (SVM™ 3000, Anton Paar) was used to measure the kinematic viscosity and density of the fuel blends following the procedure as per ASTM D7042 standard [24]. The physical properties of diesel and the 20% Karanja biodiesel/80% diesel blend (referred to as B20K) were precisely recorded, and the results are displayed in details in Table 2.

2.2. Soot particle generation

The smoke point apparatus (RAP172, installed in a fume hood, and used according to the standard ASTM D1322-08 procedure [25]) was selected for the soot generation and its collection, as the apparatus is able to produce stable flames with known fuel flow rates that allows soot particle collection at various flame heights above their smoke point. The details on the experimental setup for the smoke point analysis are provided in [31,32], and a schematic diagram of the experimental setup for flame soot collection is provided in [32,52]. Moreover, to understand the selective effect of Karanja biodiesel on metal transmission to soot particles, smoke point apparatus is preferred over diesel engine because: i) smoke point setup allows tuning combustion conditions to produce highly sooting flames, and ii) the engine-generated soots have inherent, additional metal sources such as lubricating oil and engine wear and tear impurities, while the flame-generated soot is free of such artifacts. It is worth mentioning that, while atmospheric-pressure flame setups can help in eradicating the above-mentioned engine artifacts that can affect the results, it also eliminates the effect of pressure that can affect the kinetics of soot reactions and the possible catalytic oxidation by metal nanoparticles. Ideally, a high-pressure flame would more closely represent engine conditions, though we lack such a setup. It has been shown in [26] that the pressure affected soot nanostructures mainly due to early inception of soot particles at high pressures. However, the simplicity of the ASTM standard smoke point apparatus provides an economical way to test the sooting propensity of fuels and to study the effect of fuel additives on soot production. This setup has been shown previously to predict very well the sooting trends seen in engines with diesel or gasoline blended with biofuels [27–29]. Furthermore, in [30], it was concluded by comparing flame and engine soot particles that they matched sufficiently well, and flame soot can be used as a surrogate for engine particulate matter. For further validation of the results presented in this paper using a flame setup, engine experiments can be performed in the future.

With the aid of the ASTM smoke point apparatus, the smoke points (*SP*) were measured for diesel and B20K blend fuels. Smoke point is defined as the flame height at which the sooting wings start to be visible at the tip of the diffusion flame. The threshold sooting index (*TSI*) was also calculated for the fuels by applying the equation: $TSI = a\,(MW/SP) + b$, where *MW* is the fuel molecular weight, *SP* is the smoke point in mm, and the constants, a and b are apparatus dependent, found by calibrating the apparatus with known chemical compounds. For our apparatus, their values were $a = 3.7623$ and $b = -3.7539$ (found in a previous study [24]). The observed values of smoke points and calculated TSI values are provided in Table 3 that clearly indicate the soot reduction potential of Karanja biodiesel when added to diesel.

Table 3
Smoke point and TSI values for the fuels.

Properties	Diesel	B20K Blend
Molecular weight, (g/mol)	197	336.14
Smoke Point (mm)	19	23
TSI	35.3	51.2

Soot particles were generated in the diffusion flames for diesel and B20K blend at flame height above the smoke point. In order to collect soot particles for the fuel blends at the fixed fuel flow rates, a replaceable borosilicate microfiber filter (TX40H120-WW imported from United Filtration System, USA, with 70 mm diameter, 2 μm filter pore size) was used. The particulate filter was positioned above the chimney of the smoke point apparatus so that the soot particles are captured by passing the fumes generated from the tip of the flames through the filter with the aid of a vacuum pump. After every 30–40 min, the microfiber filter was removed from the metallic cartridge and the deposited soot particles on it in the form of a cake were carefully retrieved by scrapping off gently using spatula. No chemical extraction is required, as the amount of soot deposited on the filter surface is high enough for physical extraction. The collected soot samples are then dried in an oven at a heating rate of 20 °C/min at 400 °C under N_2 flow to remove any volatiles or water components attached. Since, the pore size of the filter is the limiting factor for soot collection, it is possible that some very small particles may pass through the filter. Especially during the initial stage of soot collection, when soot layer has not developed on the filter, particles with aggregate diameter less than the filter pore size (2 μm) can penetrate through the filter and be lost during the collection process.

2.3. Measurement of fuel flow and soot collection rates

The soot production rate at a given fuel consumption rate is a good indicator of the soot suppression potential of a blending component to diesel. The fuel consumption rates for each fuel (diesel, biodiesel, and diesel/biodiesel blend) were recorded at the flame heights of 10 mm, 20 mm, and 30 mm by measuring the weight loss of the fuel in the reservoir with respect to time, as described in [33]. A fixed fuel consumption rate of 0.0008 ml/s was observed at a flame height of 20 mm for diesel and 30 mm for the biodiesel/diesel blend, as shown in Table 1S (and Fig. 1S) in the supplementary document. This chosen fuel consumption rate of 0.0008 ml/s is equivalent to 2.9 ml/h. Using the diesel density of 0.829 g/ml and B20K density of 0.84 g/ml, the fuel consumption rate in terms of mass would be almost 2.5 g/h.

At this fuel consumption rate, the soot collection rates were recorded as 0.6 mg of soot/h for pure diesel fuel and 0.55 mg of soot/h for the B20K blend.

Since the fuel consumption rate was maintained at a constant value, the soot production rate, SPR (mg of soot/g of fuel) can be calculated as follows:

$$SPR = \frac{\dot{m}_s}{\dot{m}_f} \tag{1}$$

Here, $\dot{m}_s$ is the mass (mg) of soot generated per hour and $\dot{m}_f$ is the mass (g) of fuel burnt per hour. For diesel with $\dot{m}_s$ of 0.6 mg/h and $\dot{m}_f$ of 2.5 g/h and for B20K with $\dot{m}_s$ of 0.55 mg/h and $\dot{m}_f$ of 2.5 g/h, the calculated SPR values are 0.24 and 0.22 (mg of soot/g of fuel) for diesel and B20K, respectively The SPR values indicate that soot production is

reduced by the addition of Karanja biodiesel to diesel, even while maintaining high sooting conditions in the flame. The collected samples are then subjected to ICP-MS analysis in addition to several other nanostructural characterization test such as HRTEM, XRD, and Raman spectroscopy.

2.4. ICP-MS analysis

All the samples (liquid fuels and solid soots) were digested in a high purity nitric acid solution using an industrial grade microwave oven. The digested samples were then further diluted in two stages before being analyzed in the high-performance ICP-MS. The Perkin Elmer SCIEX DRC ICP-MS model was used for this investigation. This instrument was calibrated prior to the analysis using the certified standards, and a suitable internal standard was used to compensate for the possible drift in instrument measurements. The initial masses and dilutions were factored into the software before arriving at the concentration of elements in the samples. The argon gas flow was set at a flowrate of 0.80 L/min. The fine nebulized solution was transported to a hot plasma, where it was atomized and converted to ions, which were afterwards carried to a mass spectrometer for detection. This ICP-MS technique is highly sensitive, and can attain a limit of detection of 10^{-6} mg/kg (parts per trillion) for most elements [34]. All samples were treated under identical conditions to ensure consistency. Prior to each run, the instrument underwent appropriate calibration and correction for background. Specific intensities generated from the metal constituents of interest were measured, and valid considerations were given to potential interferences and matrix effects. An aqueous certified standard (Fluka 70007; 10.00 ppb per element) was available to test the performance of the instrument on homogeneous aqueous solutions. The instrument was programmed to aspirate three aliquots of sample in quick succession and recorded the mean and deviation from the mean (relative standard deviation, RSD). Overall, the relative standard deviations of less than 5% were achieved demonstrating that the performance of the system for aqueous samples was acceptable [34].

The metal contents in the liquid fuels and diesel and biodiesel soots were recorded in the units of ppb (*ng of metal/g of soot* for soot samples, and *ng of metal/g of fuel* for liquid fuel samples). The mass of metal in soot per unit mass of fuel burnt, $M_{S/F}$ (ng of metal in soot/g of fuel burnt) to produce that soot can be calculated as follows:

$$M_{S/F} = M_{S/S} \times SPR \tag{2}$$

Here, $M_{S/S}$ is the mass of metal in soot per unit mass of soot (ng of metal in soot/mg of soot) and SPR is the soot production rate (mg of soot produced/g of fuel burnt).

This conversion was made to ensure that the metal content in the liquid fuels and the solid soots can be expressed in the same units of *ng of metal/g of fuel* so that the metal transmission rate can be calculated and compared with the TLV values. Furthermore, the percentage transmission of a metal from a fuel to soot produced from its combustion can be calculated as:

$$Metal\ \ transmission\ \ rate\ \ (\%) = \frac{M_{S/F}}{M_{F/F}} \times 100 \tag{3}$$

Here, $M_{S/F}$ is the mass of a metal in soot per unit mass of fuel burnt, and $M_{F/F}$ is the mass of metal in fuel per unit mass of fuel burnt.

3. Results and discussion

3.1. ICP-MS results on metal content distribution

Fig. 1 provides the concentrations of the trace metals in diesel fuel and its derived soot found through the ICP-MS analysis. The results indicated the presence of 21 different types of trace metals. Out of these, 17 metals were of concentrations greater than 1 ppb (presented in Fig. 1), while the remaining 4 components (Ag, Bi, U, and Th) with

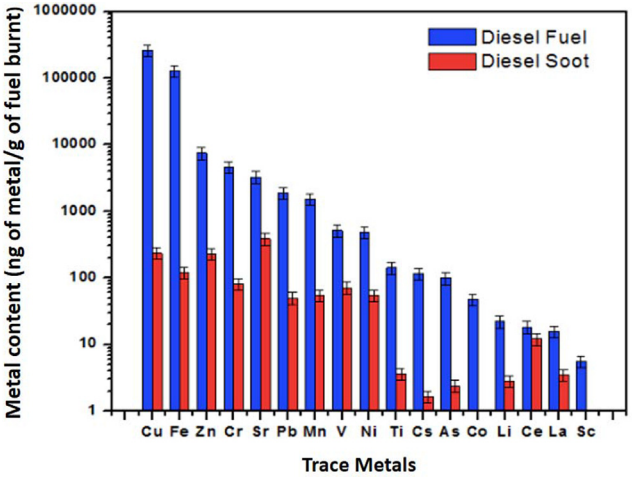

Fig. 1. Metal content in diesel fuel and its soot.

significantly low concentrations (< 1 ppb) were kept out of the scope of analysis. Copper and iron represented the two dominant metals in the diesel fuel samples with concentrations greater than 100 ppm, and were followed by Zn, Cr, Sr, Pb, and Mn, whose concentrations were in the range of 1–100 ppm. The rest of the metal components identified were having less than 1 ppm concentrations. From the metal composition in diesel soot particles, one can see that the 5 major trace metal, identified in Fig. 1, were in the range of 0.1–0.4 ppm (defined as mass of metal per unit mass of fuel burnt to produce soot particles) of the diesel combusted, with Sr having the maximum recorded concentration of 0.38 ppm.

Upon the analysis of the transmission factors of trace metals in soot particles, a significant reduction in the soot's metal content as compared with the diesel fuel was observed. As a matter of fact, the two dominant metal components that were observed in the fuel phase (i.e., Fe and Cu) were both diminished by a factor of 99.91%, which means that only 0.09% of these metal components were transmitted from the fuel phase to the soot phase. The low transmission of Fe and Cu observed in this study could be explained as follows. The oxides of the two dominant metals in fuel, Fe and Cu are known to serve as very efficient diesel soot oxidation catalysts [35,36]. Thus, the in-situ flame-deposited Cu-oxide and Fe-oxide nanoparticles on soot spherules would catalyze and enhance soot oxidation rate to either completely eliminate soot inside the flame or reduce it to very small particles. Given the small sizes of such metal nanoparticles (a few nm) or the partially oxidized soot particles containing such metal complexes, there exists a possibility that they may pass through the filter and be lost during soot collection process to indicate low transmission percentages of Cu and Fe from fuel to soot in the ICP-MS studies. While the filter pore size is 2 μm and the deposition of soot layer with time on the filter would enhance the particulate collection efficiency, the metal nanoparticles present in the gas-phase would most likely be lost. It may be possible to enhance the aggregation of metal nanoparticles by cooling the flame exhaust line near filter assembly. However, the cooling of exhaust line can also affect the flame (and soot production from it that is sensitive to temperature), and such modifications were not tested. Corbin et al. [20] reported the most abundant metal constituent of marine engine-emitted soot particles to be Vanadium (V), but our results show that Cu and Fe dominated the metal composition of diesel soot (even with their low transmission percentage), although relatively lower concentrations of V were also detected in soot. The differences in the observed results to those of Corbin et al. could be a result of differences in the fuel grade used (i.e. source metal composition in fuel) as well as the marine engine operating conditions, but these details were not available to compare the metal transmission efficiencies of the two studies. Another study on metal content of laboratory-generated soot, conducted by Bladt et al.

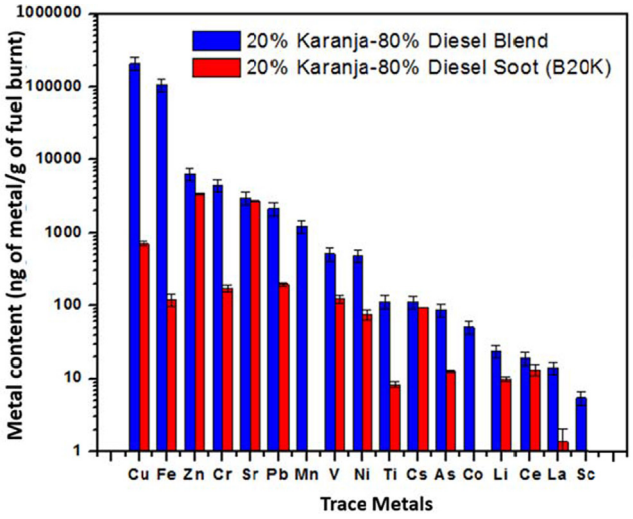

Fig. 2. Metal content in 20% Karanja biodiesel/80% diesel (B20K) fuel and its soot.

[37], found that the addition of $Fe(CO)_5$ to diesel fuel enhances Fe transmission to soot only after greater than 17% (m/m) of the metal source is added to the fuel, while the pure diesel soot did not show any presence of metal content. On the contrary, our results confirm that even pure diesel fuel contains trace metals, which are transmitted to the diesel soot. The differences in the two studies could be due to the source of diesel fuel as well as the efficiency and detection limits of ICP-MS instrument. Moreover, since the authors in [37] focused on intentional addition of known quantities of Fe to diesel, they possibly did not consider trace metal analysis of pure diesel and their transmission to diesel soot. The other detectable trace metals showed transmission from diesel fuel to soot in the range of 1–10%, while Ce revealed a high transmission of around 65%. Nonetheless, if the overall metal composition is concerned, Cu and Fe remain the dominant metal constituents of diesel soot.

In order to evaluate the influence of blending biodiesel (Karanja biodiesel) to diesel on the metal transmission efficiency into soot, further analyses were performed on metal composition of B20K fuel and soot generated from it. Fig. 2 presents the composition of trace metals in the blended fuel and its soot.

The liquid fuel blend, B20K had a very close metal composition to that of pure diesel fuel and almost identical trends. Cu and Fe remained the most dominant species detected with concentrations slightly higher than 100 ppm, and the concentrations of the rest of the metals followed similar order as the previous fuel. However, the trace metals in soot exhibited different concentrations as compared to diesel soot. Quantitatively, 0.3% of Cu and 0.11% of Fe (higher in concentration than diesel soot) were transmitted from the fuel to the B20K soot. Interestingly, some metals such as Zn, Cr, and Cs exhibited a more significant transmission rate as compared to Cu and Fe, with about 80–90% of these metals being transferred from the blended fuel to soot. For better comparison, the transmission percentages for different metals from B20K fuel to its soot were normalized with those for diesel fuel to its soot, and the calculated ratios are listed in Table 4. It is evident that the addition of Karanja biodiesel to diesel increased the metal transmission rate from fuel to soot of Zn, Sr, and Cs by a factor of approximately 17, 7, and 58, respectively, while Cu and Pd transmission increased by a factor of 3. Ce transmission remained nearly same as that in the case of pure diesel. These results were consistent over repeated experiments within the experimental error limit. In order to confirm that the increase in transmission of these metals from fuel to soot were not due to the increased metal concentration from Karanja biodiesel itself, the biodiesel was subjected to ICP-MS analysis using a similar procedure as that of other liquid fuels. The results on metal content in diesel and Karanja biodiesel are presented in Tables 2S and 3S, respectively, in the supplementary material. As evident from these tables, the Karanja biodiesel has lower metal content as compared to diesel, and therefore, the enhanced transmission of metals from B20K fuel to soot is a result of the changes induced in the combustion reactions and soot nucleation and growth mechanisms by biodiesel addition to diesel.

Table 4
Normalized metal transmission % with respect to diesel.

Element	Diesel Soot	Karanja biodiesel-Diesel soot (B20K)
Cu	1.00	3.80
Fe	1.00	1.21
Zn	1.00	17.41
Cr	1.00	2.20
Sr	1.00	7.77
Pb	1.00	3.46
Mn	1.00	0.00
V	1.00	1.73
Ni	1.00	1.35
Ti	1.00	2.89
Cs	1.00	58.51
As	1.00	6.03
Co	1.00	0.00
Li	1.00	3.17
Ce	1.00	1.06
La	1.00	0.43
Sc	1.00	0.45

It has been reported that the transmission of metals from fuel to soot during combustion may occur in the form of crystalline or amorphous metal oxides, reduced elemental form of metal, organometallic complexes or metal sulphates depending on the fuel combustion conditions [38]. Since the ICP-MS technique detects metals in their ionic forms, it cannot provide any information about the chemical and structural forms of the metals present in soot. In order to gain more insight on the enhanced transmission of metals from fuel to soot upon biodiesel addition to diesel, the influence of biodiesel on soot nanostructural disorder was studied using HRTEM, XRD and Raman analyses, and their results are presented in the subsequent sections.

3.2. HRTEM analysis

Fig. 3 shows the HRTEM micrographs at 20 and 100 nm resolution for diesel (subfigures A, A1) and B20K (subfigures B, B1) soots, respectively. The soot agglomerates, as seen in Fig. 3, are composed of primary particles that are interconnected as a result of temperature-induced sintering effect and possibly van der Waals force of attraction. Each primary particle is composed of core–shell like structure, wherein the core is formed by the small sized PAH stacks having randomly oriented disordered structure as a result of internal oxidation of soot. On the contrary, the shell is composed of long range graphitic fringes having greater degree of structural order, arranged concentrically along the periphery [39,40]. The analysis of approximately 100 primary particles using ImageJ software reveals that diesel soot (subfigure A2) has larger mean particle diameter (42.8 nm) as compared to B20K soot (subfigure B2) that has a mean particle diameter of 22.4 nm. As soot collection is carried out over several minutes to be able to have sufficient amount for characterization, this also means that particles would coagulate physically to form large aggregates. Therefore, it becomes difficult to identify primary particles from 2D HRTEM images (as there is no clear boundary between two primary particles) that limits the number of particles selected for sizing. Note that, finding the fractal dimension from such soot samples would lead to erroneous results, as such large aggregates (Fig. 3A1, B1) may have formed on the filter (and not actually present as such large aggregates in the flame). That's why, for fractal dimension studies, soot is deposited quickly for a few milliseconds only on a TEM grid and analyzed.

The addition of oxygenated biodiesel to diesel results in an

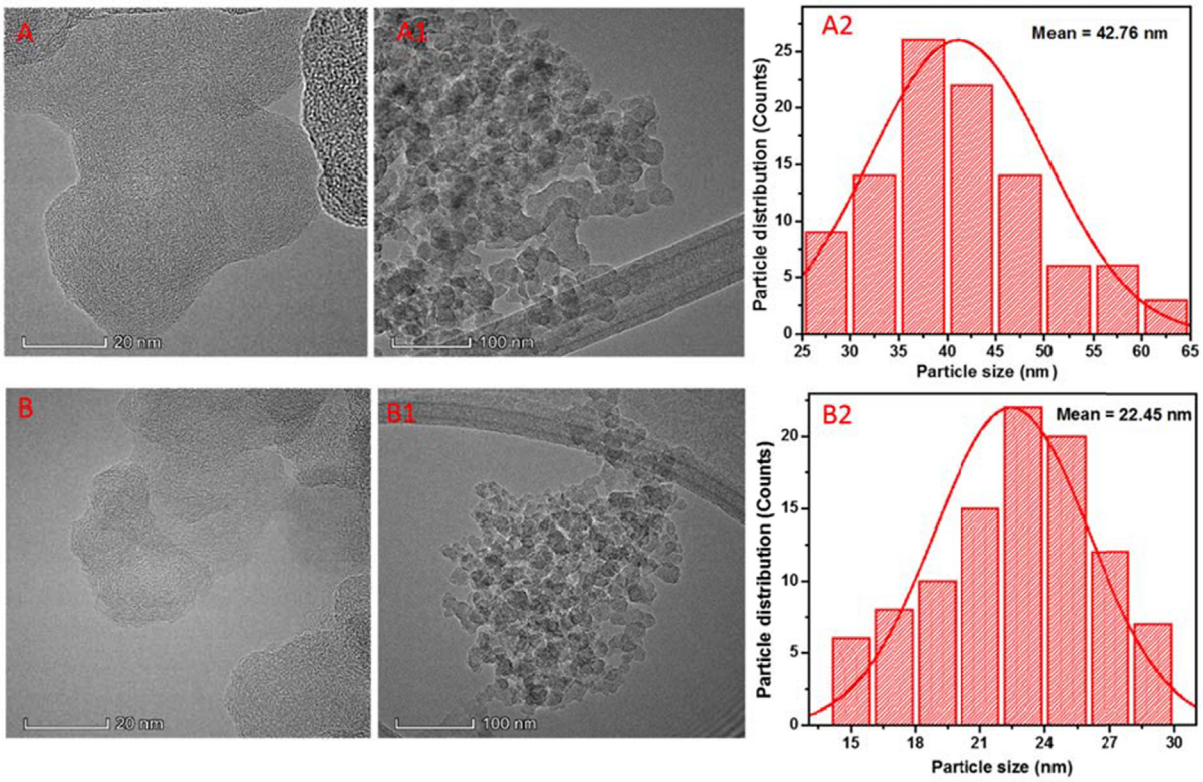

Fig. 3. HRTEM images of (A, A1) Diesel soot and (B, B1) B20K soot along with their particle size distribution histograms (A2 and B2, respectively).

enhanced fuel oxidation, as the fuel-bound oxygen provides homogeneous and improved oxygen: fuel ratio [42]. Thus, the size of primary particles decreases as their formation and growth gets affected, though the presence of a large number of small soot particles in the flame of blended fuel may increase the soot surface area. Moreover, the enhanced oxygen:fuel ratio may also enhance the internal oxidation of soot, resulting in a higher crystal structure disorder within soot [41].

For the quantitative information on the microstructural disorder in soot, the HRTEM micrographs were analyzed using a Matlab code, constructed based on the algorithm of Yehliu et al [42], to determine fringe length and tortuosity index. In this method, the high-resolution image of primary particle is first subjected to a negative transformation, stated as $I_{negative} = L\text{-}1\text{-}I_{original}$, with L being the discrete intensity levels (approx. 256 per image), and $I_{original}$ is the image pixel value before transformation. Multiple images are selected, and operations such as Gaussian filtering, histogram equalization, and Tophat transformation are performed, which eliminate errors due to non-homogeneous illumination and improve the fringe contrast across the image. The skeletonization of the fringe structure is achieved using parallel thinning algorithm [43], which allows eliminating small branches from the parent fringe skeleton. With reference to these branch points, mean fringe length and tortuosity were determined in all directions using the Matlab code. For further details on the algorithm and equations used, the reader is directed to reference [42]. The analyzed fringe microstructures for diesel and B20K soots are shown in Fig. 4, and the calculated mean fringe length and tortuosity values are provided in Table 5. It is evident from the table that the B20K soot has a significantly greater fringe structure disorder, with shorter mean fringe length of 2 nm and greater mean fringe tortuosity of 1.58 as compared diesel soot, which has mean fringe length of 2.3 nm and tortuosity of 1.36. The shorter fringe lengths and greater tortuosity (caused by the presence of entrapped 5-member rings in aromatic structures [44,45]) in B20K soot indicates an enhanced internal oxidation of soot (which convert 6-membered ring to 5-membered ring) and/or reduced soot growth. Such disorder in soot nanostructure is known to induce greater reactivity of soot particles with oxidants such as O_2 and radicals [24], and may even react chemically with metal ions present in the flame to form metal-oxo complexes with active centers on the soot surface or metal oxide particles trapped in soot agglomerates. Such a possibility could result in enhanced transmission of metal ions from fuel to soot with higher reactivity and larger surface area. Miller et al. [46] studied the effect of $Fe(CO)_5$ doping of diesel fuel in a diesel engine. They observed through TEM analysis that, at significantly higher Fe concentration (> 1000 PPM), when the Fe/C ratio exceeds 0.013, the Fe vapors starts to condense and form tiny particles on the soot spherules, while lower Fe/C ratio results in soot structure similar to pure diesel soot. They did not evaluate its effect on the fringe and crystal structure disorder of soot. Moreover, in their study, several factors such as the selectivity of intentionally added $Fe(CO)_5$ structure to condensation and nucleation on soot, complexity of engine conditions such as high temperature, pressure, added metal sources such as lubricating oil impurities, and the engine wear and tear could also result in the increased metal concentration in soot, and hence, the effect of metal transmission exclusively from fuel to soot is difficult to estimate.

Considering all the above factors, it can be concluded that the lower metal/carbon ratio in the fuel used in this work, the absence of any engine artifacts that can enhance metal content in soot (through the use of laminar diffusion flame), and the in-situ catalytic oxidation of soot by metal oxide particles leading to its subsequent loss, could be responsible for the absence of obvious metal oxide nanoparticles in the TEM images of soot, while their presence was evident through ICP-MS analysis.

3.3. X-ray diffraction analysis

The diesel and B20K soot samples were subjected to X-ray diffraction analysis, and the results are shown in Fig. 5. No characteristic peaks of the metals/metal oxides (detected in ICP-MS experiments) were observed in the XRD pattern, possibly due to their low concentrations that is below the detection limit of this technique. As reported by Bladt et al. [37], even at high metal concentrations, the metal

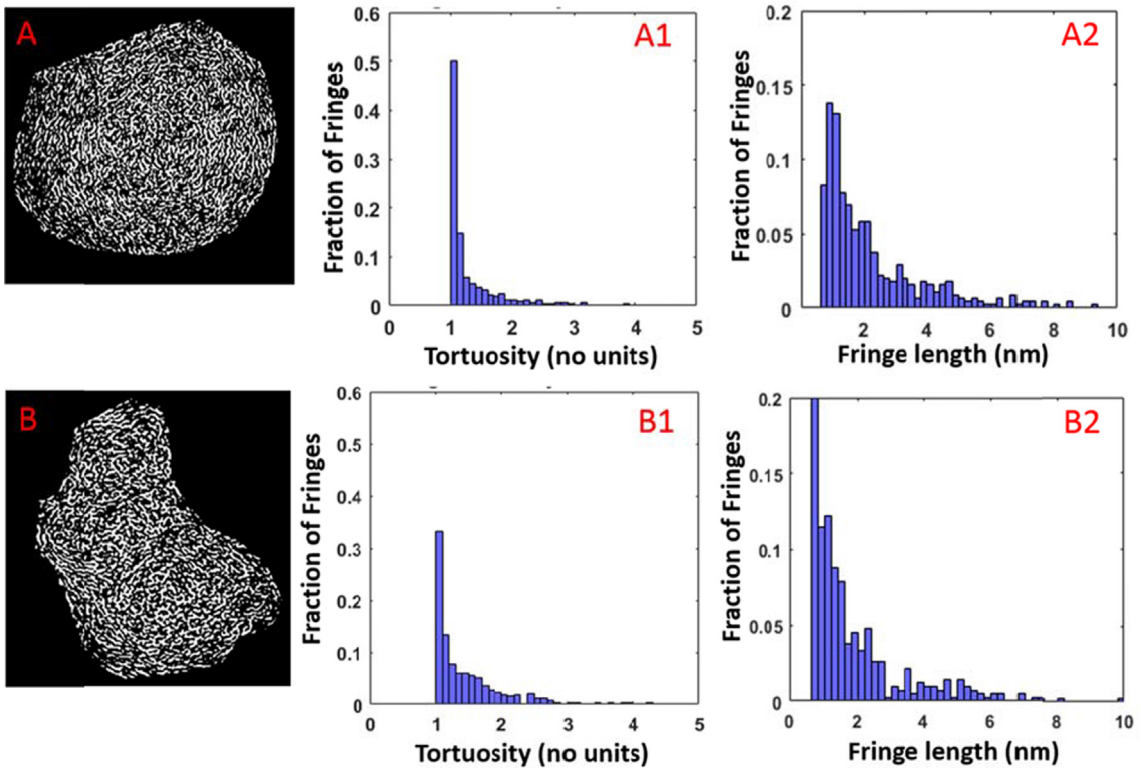

Fig. 4. Matlab processed microstructure analysis depicting fringe length and tortuosity index distribution of A) diesel soot and B) B20K soot.

Table 5
Soot nanostructural parameters obtained from HRTEM, XRD and Raman analysis.

Sample Properties	Diesel soot	B20K soot
HRTEM results		
Mean fringe length	2.3 nm	2.0 nm
Mean fringe tortuosity	1.36	1.58
Primary particle diameter	42.7 nm	22.1 nm
XRD results		
Interlayer spacing, d_{002}	0.362 nm	0.371 nm
Nano-crystallite height, L_c	1.207 nm	1.071 nm
Nano-crystallite width, L_a	3.02 ± 0.5 nm	2.95 ± 0.5 nm
L_c/d_{002} (no. of layers, N)	3.33	2.89
Raman results		
I_{D1}/I_G ratio	1.26 ± 0.05	1.51 ± 0.05
Lattice width, L_a	3.4 ± 0.5 nm	2.87 ± 0.5 nm

oxides trapped in soot structure are highly amorphous in nature and therefore do not exhibit characteristic peaks in XRD unlike crystalline oxides. Nonetheless, the characteristics peaks of carbon soot at 2θ values of around 25° and 44° were observed. The first peak at 25° is assigned to the (0 0 2) plane, which provides the information about the interlayer spacing and the thickness of the PAH stack. The peak at 44° is due to the (1 0 0) plane, and contains information about the average size of the PAHs in soot. The quantification of interlayer spacing (d_{002}) was performed using the Bragg's law (equation E4), the nano-crystallite height (L_c) was obtained using Scherer formula (Equation E5), while the nano-crystallite width or average size of the PAH stack (L_a) was calculated using Equation E6.

$$d_{002} = \frac{\lambda}{2sin\theta_{002}} \tag{4}$$

$$L_c = \frac{0.9\lambda}{B_{002}cos\theta_{002}} \tag{5}$$

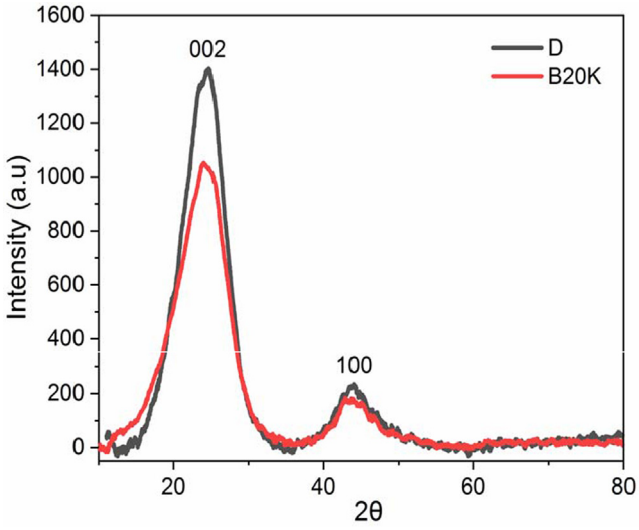

Fig. 5. Powder X-ray diffractogram of Diesel soot and B20K soot.

$$L_a = \frac{1.84\lambda}{B_{100}cos\theta_{100}} \tag{6}$$

In the above equations, λ is the wavelength of X-ray (0.154 nm for Cu Kα), θ_{002} and θ_{001} are the Braggs angles, and the full width at half maximum (FWHM) for the two peaks are B_{002} and B_{100}. The Braggs angles and the FWHM were obtained via Gaussian fitting of the respective peaks using Matlab software. It is evident from the values listed in Table 5 that the interlayer separation between the graphitic planes (d_{002}) increases to 0.371 nm (B20K soot) from 0.362 nm (diesel soot), while the crystallite width, L_a decreases to 2.95 nm (B20K soot) from 3.01(diesel soot). The number of graphitic layers (L_c/d_{002}) in a given PAH stack decreases to 2.89 in case of B20K soot as compared to 3.33 in case of diesel soot. Such a reduction in PAH stack size is known to make

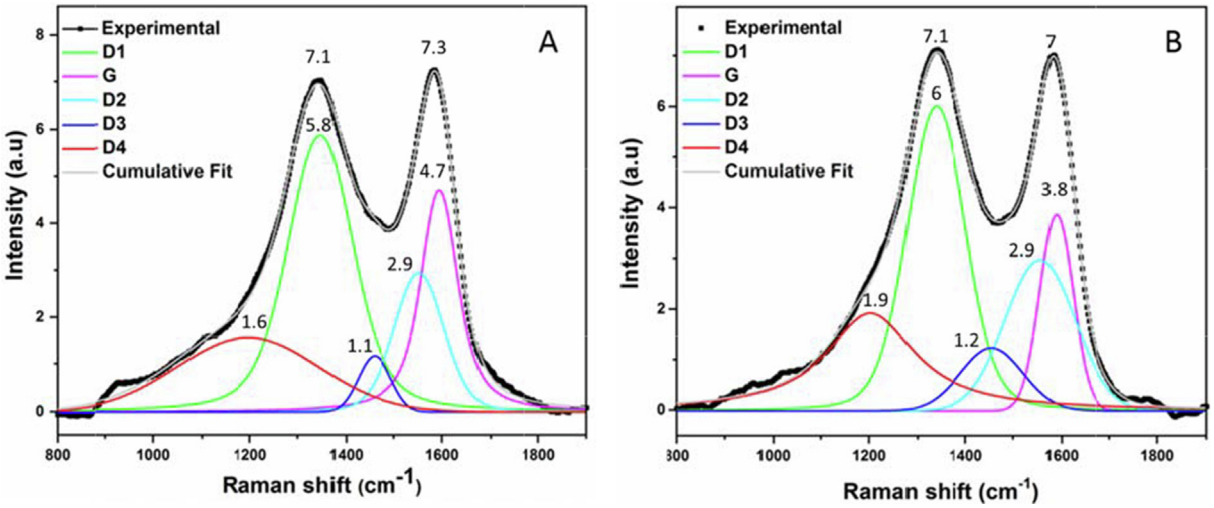

Fig. 6. Raman spectra of A) Diesel soot and B) B20K soot. Peak intensities are marked.

the soot amorphous and increase the effective surface area of the soot particles, and the increased interlayer spacing results in greater exposure of reactive edge carbon atoms compared to the less reactive basal carbon atoms [40]. These changes increase the reactivity of the B20K soot particles, which could react/trap greater number of metal/metal oxide particles during the combustion of B20K fuel blend compared to diesel, resulting in increased metal transmission rate. The degree of crystal disorder in soot plays an important role in the reactivity of soot particles with oxidants, radicals, and even indirectly with living cells when emitted to the environment and inhaled [47]. Therefore, the diesel and B20K soot samples were further subjected to Raman analysis to estimate the ratio of disordered PAH layers to the ordered graphitic layers, as presented in the next section.

3.4. Raman analysis

Two characteristic Raman bands, one at 1350 cm^{-1} (called as the D band) and the second one at 1590 cm^{-1} (known as the G band) were observed in the Raman spectrum, as shown in Fig. 6. The D band represents the most disordered graphitic core and is also associated with the aliphatic content of soot particles. On the other hand, the G band represents the well-ordered graphitic structure mostly along the periphery of the shell structure of soot [48,49]. Each Raman spectra consisted of 200 data points that were used for fitting. Three different regions per soot sample were analysed for consistency, and the error bars reported in the results were calculated accordingly. Raman spectra were analysed using the 5-curve deconvolution model. Voigt function were used to fit the raw data, as suggested in [50]. The fitted peaks were coded as D1 = 1345 cm^{-1}, D2 = 1560 cm^{-1}, D3 = 1445 cm^{-1}, D4 = 1220 cm^{-1}, and G = 1590 cm^{-1}. The D2 peak is associated with lattice vibrations, while D3 represents the highly amorphous carbon in soot samples. Unlike Bladt et al. [37], who observed a split in the D4 band into two single peaks that increased with Fe content in soot, the Raman spectra of both diesel and B20K soots in this work exhibited similar broad shoulders of the D4 band without any split. The retainment of the D4 band in the present study could be due to low metal concentration in soot (in ppb level), while in [37], the large quantities of Fe were added to the fuel to see its effect. Such excessive external addition of Fe in fuel could induce artifacts in the metal transmission analysis, as these metals could act as nuclei for soot inception, condensation, growth and its internal oxidation that can further alter soot nanostructure. Moreover, at high Fe addition up to 60% (m/m), additional peaks around 600–800 cm^{-1} were observed by Baldt et al. due to the presence of Fe_2O_3, which were completely missing in soots analysed in the present study.

Nonetheless, soot nanostructure was studied by comparing first ordered graphitic G band intensity and the D band intensity. The ratio of the intensities of D1 to G band (I_{D1}/I_G) represents the magnitude of discontinuity and disorder in graphene layers present in soot [50,40], which is equated to the lattice width (L_a) through Knight and White equation (Equation E7) [51]. A proportionality constant of 4.4 for the excitation wavelength of 515 nm, as suggested in [44,45], is used. The obtained I_{D1}/I_G and L_a values are listed in Table 5.

$$L_a = 4.4\left(\frac{I_{D1}}{I_G}\right)^{-1} \quad (7)$$

The I_{D1}/I_G value for diesel soot was 1.26, while in the case of B20K soot, it was 1.51. The higher value in B20K soot indicates a greater disordered graphitic structure in it. The lower value of L_a in case B20K soot (2.87 nm) compared to diesel soot (3.4 nm) are in good agreement with the XRD results, and further confirms that the addition of Karanja biodiesel to diesel enhances the internal oxidation of soot particles resulting in a greater disordered fringe structure, and smaller PAH and particle size, which makes the B20K soot more reactive and thus could possibly explain the enhanced transmission rate of metal/metal oxides from blended fuel to the soot.

The addition of Karanja biodiesel, which is composed of long chain methyl ester of fatty acids, to diesel could impart changes in the surface functional groups of the small sized PAH nuclei to enhance their crystal disorder (as observed above, possibly by adding aliphatic chains) and reactivity towards metal ions such as Zn, Sr, Cs, and Pb, which could explain the enhancement in the transmission factor of these metals. Further analysis using X-ray photoelectron spectroscopy could possibly provide greater insight in this aspect. However, due to the lack of instrumental facility, such an investigation could not be conducted at this stage. More importantly, the duel combination of greater metal/metal oxide transmission from Karanja blended diesel fuel to soot and the increased microstructural disorder and smaller particle size of B20K soot makes the biodiesel-diesel soot highly hazardous, if emitted directly to the environment.

4. Conclusion

A detailed investigation on the concentrations of trace metals in fuels (diesel and 20% Karanja biodiesel/80% diesel blend) and their soots and on the nanostructural characterization of soot particles was presented. It was observed that transition metals were the major metal constituents of diesel fuel, which got transmitted to soot during combustion. Although the concentrations of Cu and Fe were highest among

all metals in diesel fuel and its soot, their transmission from fuel to soot was only about 0.09%, possibly because their oxides are excellent soot oxidation catalysts that may have enhances soot oxidation and returned to the gas phase. Interestingly, the addition of Karanja biodiesel to diesel enhanced the transmission of environmentally toxic metals such as Zn, Sr, Cs, and Pb to soot. The normalized transmission factor, defined as the ratio of the transmission rate from diesel to its soot (%) and the transmission rate from blended fuel to its soot (%), for Zn, Sr, Cs and Pb increased by the factors of 17, 7, 58, and 3, respectively. To understand the trends of metal transmission, the HRTEM, XRD, and Raman spectra of soot samples were analyzed to quantify soot nanostructural parameters. The addition of Karanja biodiesel to diesel reduced primary particle diameter and fringe length and increased structural disorder with enhanced fringe tortuosity in soot that can increase its reactivity towards oxidants, radicals, and metal ions. Such an increased reactivity could enhance the transmission of metals/metal oxides from gas-phase to soot during the combustion of the blended fuel. The combination of greater degree of metal/metal oxide transmission from Karanja-biodisel blended diesel fuel to soot and the increased microstructural disorder and reactivity makes soots from biodiesel-diesel blend highly hazardous for living beings. Therefore, improved extraction and distillation strategies to reduce the toxic metal content in fossil as well as renewable fuels would be essential to reduce the impact of their combustion on human health and the environment.

CRediT authorship contribution statement

Pranay P. Morajkar: Data curation, Formal analysis, Investigation, Visualization, Writing - review & editing. **Moataz K. Abdrabou:** Data curation, Formal analysis, Investigation, Visualization, Writing - original draft. **Abhijeet Raj:** Conceptualization, Funding acquisition, Project administration, Resources, Supervision, Writing - review & editing. **Mirella Elkadi:** Funding acquisition, Project administration, Resources. **Sasi Stephen:** Data curation, Formal analysis, Investigation. **Mohamed Ibrahim Ali:** Resources, Writing - review & editing.

Declaration of Competing Interest

The authors declare that they have no known competing financial interests or personal relationships that could have appeared to influence the work reported in this paper.

Acknowledgement

The authors would like to acknowledge the financial support received from Khalifa University of Science & Technology (CIRA-2018-99) U.A.E and instrumental facilities support of Goa University, India (via DST/IMRCD/INNO-INDIGO/BioCFD/2017(G)) in order to accomplish this work. This publication is based upon work supported by the Khalifa University of Science and Technology under Award No. RC2-2018-024.

Appendix A. Supplementary data

Supplementary data to this article can be found online at https://doi.org/10.1016/j.fuel.2020.118631.

References

[1] Fatih Birol, “IEA (2019), World Energy Outlook 2019, IEA, Paris,” 2019. .
[2] Singh D, Singal SK, Garg MO, Maiti P, Mishra S, Ghosh PK. Transient performance and emission characteristics of a heavy-duty diesel engine fuelled with microalga Chlorella variabilis and Jatropha curcas biodiesels. Energy Convers Manag 2015;106:892–900.
[3] Hosseinzadeh-Bandbafha H, Tabatabaei M, Aghbashlo M, Khanali M, Demirbas A. A comprehensive review on the environmental impacts of diesel/biodiesel additives. Energy Convers Manag 2018;174(June):579–614.
[4] Basavaraj G, Rao PP, Reddy CR, Kumar AA, Rao PS, Reddy BVS. A review of national biofuel policy in india: a critique- need for promotion of alternative feedstocks. J Biofuels 2012;3(2):65.
[5] Howell S. Biodiesel Progress: ASTM Specifications and 2nd Generation Biodiesel. Biodiesel board: Natl; 2007.
[6] Aghbashlo M, Tabatabaei M, Mohammadi P, Pourvosoughi N, Nikbakht AM, Goli SAH. Erratum: Improving exergetic and sustainability parameters of a di diesel engine using polymer waste dissolved in biodiesel as a novel diesel additive (Energy Conversion and Management (2015) 105 (328–337)). Energy Convers Manag 2016;109:213.
[7] Qi DH, Geng LM, Chen H, Bian YZ, Liu J, Ren XC. Combustion and performance evaluation of a diesel engine fueled with biodiesel produced from soybean crude oil. Renew Energy 2009;34(12):2706–13.
[8] Fenimore CP. Formation of nitric oxide in premixed hydrocarbon flames. Symp Combust 1971;13(1):373–80.
[9] Ahmed M, Guo X, Zhao XM. Determination and analysis of trace metals and surfactant in air particulate matter during biomass burning haze episode in Malaysia. Atmos Environ 2016;141:219–29.
[10] Elkadi M, Pillay A, Fok SC, Feghali F, Bassioni G, Stephen S. Depth profiling (ICP-MS) study of toxic metal buildup in concrete matrices: Potential environmental impact. Sustainability 2010;2(10):3258–69.
[11] Lee DG, Miller A, Park KH, Zachariah MR. Effects of trace metals on particulate matter formation in a diesel engine: Metal contents from ferrocene and lube oil. Int J Automot Technol 2006;7(6):667–73.
[12] Tchounwou PB, Yedjou CG, Patlolla AK, Sutton DJ. Heavy metal toxicity and the environment. EXS 2012;101:133–64.
[13] Amedro D. et al., “HOx and ROx Radicals in Atmospheric Chemistry,” in Disposal of Dangerous Chemicals in Urban Areas and Mega Cities, 2013, pp. 77–92.
[14] Singh JP, Thakur SN. Laser-Induced Breakdown Spectroscopy. Elsevier Science, 2007.
[15] Geiger A, Cooper J. “Overview of Airborne Metals Regulations, Exposure Limits, Health Effects, and Contemporary Research,” Contin. (Minneap. Minn), vol. 22, no. 1, pp. 285–286, 2016.
[16] Utsunomiya S, Jensen KA, Keeler GJ, Ewing RC. Direct Identification of Trace Metals in Fine and Ultrafine Particles in the Detroit Urban Atmosphere. Environ Sci Technol 2004;38(8):2289–97.
[17] Hofmann W. Modelling inhaled particle deposition in the human lung—A review. J Aerosol Sci 2011;42(10):693–724.
[18] Ghio AJ. Metals associated with both the water-soluble and insoluble fractions of an ambient air pollution particle catalyze an oxidative stress. Inhal. Toxicol. Jan. 1999;11(1):37–49.
[19] Lee BK, Hieu NT. Seasonal Variation and Sources of Heavy Metals in Atmospheric Aerosols in a esidential Area of Ulsan, Korea. Aerosol Air Qual Res 2011;11(6):679–88.
[20] Corbin JC, et al. Trace Metals in Soot and PM2.5 from Heavy-Fuel-Oil Combustion in a Marine Engine. Environ Sci Technol 2018;52(11):6714–22.
[21] Dore AJ, et al. Quantifying missing annual emission sources of heavy metals in the United Kingdom with an atmospheric transport model. Sci Total Environ 2014;479–480(1):171–80.
[22] Shiraiwa M, Selzle K, Pöschl U. Hazardous components and health effects of atmospheric aerosol particles: reactive oxygen species, soot, polycyclic aromatic compounds and allergenic proteins. Free Radic. Res. Aug. 2012;46(8):927–39.
[23] ASTM:D975-15b, “Standard specification for diesel fuel oils,” ASTM Int., pp. 1–25, 2015.
[24] Alrefaai MM, Guerrero Peña GDJ, Raj A, Stephen S, Anjana T, Dindi A, “Impact of dicyclopentadiene addition to diesel on cetane number, sooting propensity, and soot characteristics,” Fuel, vol. 216, no. November 2017, pp. 110–120, 2018.
[25] Watson RJ, Botero ML, Ness CJ, Morgan NM, Kraft M. An improved methodology for determining threshold sooting indices from smoke point lamps. Fuel 2013;111:120–30.
[26] Commodo M, Karataş AE, De Falco G, Minutolo P, D’Anna A, Gülder ÖL. On the effect of pressure on soot nanostructure: A Raman spectroscopy investigation. Combust Flame 2020;219:13–9.
[27] Gogoi B, et al. Effects of 2,5-dimethylfuran addition to diesel on soot nanostructures and reactivity. Fuel 2015;159:766–75.
[28] Guerrero Peña GDJ, Hammid YA, Raj A, Stephen S, Anjana T, Balasubramanian V. On the characteristics and reactivity of soot particles from ethanol-gasoline and 2,5-dimethylfuran-gasoline blends. Fuel 2018;222:42–55.
[29] Kareem MO, Pena GDJG, Raj A, Alrefaai MM, Stephen S, Anjana T. Effects of neem oil-derived biodiesel addition to diesel on the reactivity and characteristics of combustion-generated soot. Energy Fuels 2017;31(10):10822–32.
[30] Maricq MM. Examining the relationship between black carbon and soot in flames and engine exhaust. Aerosol Sci Technol 2014;48(6):620–9.
[31] Guerrero Peña GDJ, et al. Effects of methyl group on aromatic hydrocarbons on the nanostructures and oxidative reactivity of combustion-generated soot”. Combust Flame 2016;172:1–12.
[32] Abdrabou MK, Morajkar PP, Guerrero Peña GDJ, Raj A, Elkadi M, Salkar AV. Effect of 5-membered bicyclic hydrocarbon additives on nanostructural disorder and oxidative reactivity of diffusion flame-generated diesel soot. Fuel 2020;275:117918. https://doi.org/10.1016/j.fuel.2020.117918.
[33] Peña GDJG, et al. Physicochemical properties of soot generated from toluene diffusion flames: Effects of fuel flow rate. Combust Flame 2017;178:286–96.
[34] Pillay AE, et al. A comparison of trace metal profiles of neem biodiesel and commercial biofuels using high performance ICP-MS. Fuel 2012;97:385–9.
[35] Wagloehner S, Baer JN, Kureti S. Structure–activity relation of iron oxide catalysts in soot oxidation. Appl. Catal. B Environ. 2014;147:1000–8.

[36] López-Suárez FE, Bueno-López A, Illán-Gómez MJ, Adamski A, Ura B, Trawczynski J. Copper Catalysts for Soot Oxidation: Alumina versus Perovskite Supports. Environ Sci Technol 2008;42(20):7670–5.
[37] Bladt H, et al. Impact of fe content in laboratory-produced soot aerosol on its composition, structure, and thermo-chemical properties. Aerosol Sci Technol 2012;46(12):1337–48.
[38] Chernyshev VV, et al. Morphological and chemical composition of particulate matter in buses exhaust. Toxicol. Reports 2019;6(December 2018):120–5.
[39] Botero ML, Chen D, González-Calera S, Jefferson D, Kraft M. HRTEM evaluation of soot particles produced by the non-premixed combustion of liquid fuels. Carbon N. Y. 2016;96:459–73.
[40] Morajkar PP, et al. Effects of Camphor Oil Addition to Diesel on the Nanostructures and Oxidative Reactivity of Combustion-Generated Soot. Energy Fuels 2019;33(12):12852–64.
[41] Lapuerta M, Rodríguez-Fernández J, Sánchez-Valdepeñas J. Soot reactivity analysis and implications on diesel filter regeneration. Prog Energy Combust Sci 2020;78.
[42] Yehliu K, Vander Wal RL, Boehman AL. Development of an HRTEM image analysis method to quantify carbon nanostructure. Combust Flame 2011;158(9):1837–51.
[43] Lam L, Lee S, Suen CY. Thinning methodologies-a comprehensive survey. IEEE Trans Pattern Anal Mach Intell 1992;14(9):869–85.
[44] Raj A, Yang SY, Cha D, Tayouo R, Chung SH. Structural effects on the oxidation of soot particles by O2: Experimental and theoretical study. Combust Flame 2013;160(9):1812–26.
[45] Raj A. Structural effects on the growth of large polycyclic aromatic hydrocarbons by C2H2. Combust Flame 2019;204:331–40.
[46] Miller A, Ahlstrand G, Kittelson D, Zachariah M. The fate of metal (Fe) during diesel combustion: Morphology, chemistry, and formation pathways of nanoparticles. Combust Flame 2007;149(1):129–43.
[47] Kocbach Bølling A, et al. Health effects of residential wood smoke particles: the importance of combustion conditions and physicochemical particle properties. Part Fibre Toxicol Nov. 2009;6:29.
[48] Sadezky A, Muckenhuber H, Grothe H, Niessner R, Pöschl U. Raman micro-spectroscopy of soot and related carbonaceous materials: Spectral analysis and structural information. Carbon N. Y. Jul. 2005;43(8):1731–42.
[49] Salamanca M, Mondragón F, Agudelo JR, Benjumea P, Santamaría A. Variations in the chemical composition and morphology of soot induced by the unsaturation degree of biodiesel and a biodiesel blend. Combust Flame Mar. 2012;159(3):1100–8.
[50] Catelani T, Pratesi G, Zoppi M. Raman characterization of ambient airborne soot and associated mineral phases. Aerosol Sci Technol 2014;48(1):13–21.
[51] Escribano R, Sloan JJ, Siddique N, Sze N, Dudev T. Raman spectroscopy of carbon-containing particles. Vib Spectrosc Nov. 2001;26(2):179–86.
[52] Guerrero Peña GDJ, Hammid YA, Raj A, Stephen S, Anjana T, Balasubramanian V. On the characteristics and reactivity of soot particles from ethanol-gasoline and 2,5-dimethylfuran-gasoline blends. Fuel 2017, 2018,;222(November):42–55.